

# Analysis and Optimization of Semicircular and Straight Lobe Viscous Pumps

M. Mainland<sup>1</sup>

I. Green  
Mem. ASME

The George W. Woodruff School of  
Mechanical Engineering,  
Georgia Institute of Technology,  
Atlanta, GA 30332-0405

*A viscous pump design that is capable of producing higher flow rates than a viscous pump previously introduced by Etsion and Yaier (1988) is developed and investigated. The key to the new design is straight lobes as opposed to the semicircular lobes of the previous design. The geometry of the straight lobes does not lend itself to as straightforward a solution as the semicircular lobe analysis. Approximations are made and then verified using upper and lower shape factor bounds and finite element analyses. Lobe geometry for each lobe design is optimized to produce maximum pumping capacity. The results of the optimization show that the straight lobe pump is theoretically superior to the semicircular lobe pump.*

## Introduction

A new concept viscous pump was first introduced by Etsion and Yaier (1988). The pumping mechanism was provided by a semicircular lobe design. In the current work, a more flow-efficient straight lobe design is investigated. Important features of these pumps include nonpulsatile flow rate and discharge pressure, a linear flow-pressure relationship, easy adaptability to a needed flow-pressure operating point, and no need for dynamic seals or valves.

The viscous pump is advantageous for applications requiring easy and accurate flow control, such as in steady flow metering pumps, or pumping jobs that require high levels of cleanliness, e.g., blood and other biofluid pumps. This is because there is no contact between rotor and stator in the fluid flow path, nor does this fluid face any lubricating fluids. The viscous pump can produce flow rates comparable to peristaltic pumps, but avoids the potentially damaging normal force created by the squeezing action of peristaltic pumps. The viscous pump is comparable to other rotary pumps such as screw or gear pumps but avoids the local pressure build up at gear matings that can be damaging to the process fluid. In cases of pumping slurries containing abrasive crystals, such as aluminum dioxide (which has a hardness close to that of a diamond), serious damage to the gear surfaces is highly likely. The viscous pump can pump such viscous slurries without being damaged by the abrasive crystals, providing that the gaps between stator lobes and rotor are made bigger than the diameter of the crystal.

Other pumps that take advantage of the viscosity of the fluid to transfer energy from the rotor to the fluid have been introduced in the literature. The shear-force pump (Hasinger

and Kehrt, 1963) has closely spaced rotor disks that accelerate the fluid radially outward. Somewhat extensive work has been done in the area of spiral groove viscous pumps (e.g., Sato et al., 1990), which also have typical applications in bearings and seals. An analytical and experimental investigation of flow between a stationary disk and grooved rotating disk was performed by Missimer and Johnson (1982). The well known narrow groove theory introduced by Vohr and Pan (1969) forms the basis for many investigations related to spiral grooves (e.g., Hsing, 1972 and 1974). A viscous pump with shrouded Rayleigh steps was studied by Sato et al. (1988).

The idea for the type of viscous pump under study in this work originated as a new concept for a zero-leakage noncontacting mechanical face seal proposed by Etsion (1984). The idea of the semicircular lobe design was then reformulated as an idea for a viscous pump (Etsion and Yaier, 1988). An optimization of pump geometry for maximum pump efficiency was performed on a limited basis. An experimental investigation of a semicircular lobe viscous pump was performed by Green et al. (1989). That work proved that the semicircular lobe design provides a feasible pumping mechanism. In the current work, the semicircular lobes are replaced by straight lobes. When the two designs are optimized, the straight lobes prove to have the potential of producing significantly higher flow rates at a given discharge pressure.

## Operating Principles

In semicircular lobe pump, the rotor and stator are parallel circular disks separated by the process fluid. Specially designed circular lobes, shown in Fig. 1, protrude from the surface of the stator and make a small gap,  $c$ , and a larger gap,  $C$ , with a flat disk rotor. The gaps  $C$  and  $c$  are in the order of microns. The fluid is sheared by the rotor and is dragged by viscous forces in a circumferential direction with the rotor.

The design of the lobes is the key to obtaining a net pumping action. Referring again to Fig. 1, the shear induced flow

<sup>1</sup>Currently at University of Illinois at Urbana-Champaign, Department of Mechanical and Industrial Engineering, Urbana, IL 61801.

Contributed by the Tribology Division of THE AMERICAN SOCIETY OF MECHANICAL ENGINEERS and presented at the STLE/ASME Tribology Conference, St. Louis, Mo., October 13-16, 1991. Manuscript received by the Tribology Division February 8, 1991; revised manuscript received June 1991. Paper No. 91-Trib-39.

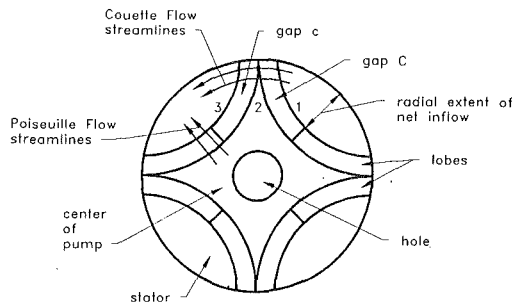


Fig. 1 Stator of semicircular lobe viscous pump

(Couette flow) is represented by streamlines that are concentric circumferential lines in the direction of the rotor rotation. That flow is proportional to the radial extent and the gap height. Because of the gap height difference,  $C-c$ , more fluid is sheared into the center of the pump from point 1 to point 2 than is allowed to exit from point 2 to point 3. The fluid in the center of the pump can exit through a hole in the center of the stator. If the flow through the hole is restricted (e.g., by a valve) then pressure is built up at the pump center. Thus, if that pressure is greater than the pressure of the fluid surrounding the rotor and stator, then a pressure-gradient induced flow (Poiseuille flow) will travel from the center of the pump, across the lobes, to the inlet low pressure zone. Maximum pumping efficiency occurs when the geometry is prescribed such that the net inward Couette flow is maximized while the Poiseuille flow (leakage losses) is minimized.

The Reynolds equation is used to model the flow field in the pump. Although this equation can be solved using a closed form integration for the semicircular lobe geometry, some approximations must be made to account for the more complex geometry of the straight lobes. The simplifications made will be justified by comparing the simplified analytical model against upper and lower bound shape factors and then to a finite element computational model. The equations will then be optimized for geometry that will produce maximum pumping efficiency. Finally, the optimized results of both the semicircular and straight lobe designs will be compared.

### Analysis

For an isothermal, steady, incompressible fluid film, and a boundary moving in the  $x$  direction at a velocity  $U$ , the Reynolds equation is

$$\frac{\partial}{\partial x} \left( h^3 \frac{\partial p}{\partial x} \right) + \frac{\partial}{\partial y} \left( h^3 \frac{\partial p}{\partial y} \right) = 6\mu U \frac{\partial h}{\partial x} \quad (1)$$

### Nomenclature

$c$  = small clearance between rotor and stator  
 $C$  = large clearance between rotor and stator  
 $h$  = fluid film thickness (clearance)  
 $L$  = length dimension for various geometries  
 $p$  = pressure  
 $P$  = differential discharge pressure  
 $q$  = flow per unit length  
 $Q$  = dimensional volumetric flow  
 $Q'$  = dimensionless volumetric flow, Eq. (9)  
 $Q'_{c0}$  = dimensionless volumetric flow for zero clearance, Eq. (22)

$R$  = radial coordinate measured from stator center  
 $r$  = general radial coordinate  
 $s$  = lobe step height,  $C-c$   
 $S$  = general path coordinate  
 $S$  = shape factor  
 $S'$  = operating conditions parameter,  $\frac{\pi P}{12 \mu \omega} \left( \frac{c}{R_o} \right)^2$   
 $\alpha$  = variable lobe angle  
 $\beta$  = lobe angle determined by number of lobes  
 $\delta$  = dimensional V-lobe thickness  
 $\Delta r$  = dimensional semicircular lobe thickness

$\mu$  = absolute viscosity of fluid  
 $\xi$  = dimensionless lobe thickness,  $\Delta r/R_o$  or  $\delta/R_o$   
 $\sigma$  = dimensionless step height,  $s/c$   
 $\omega$  = angular velocity of rotor

### Subscripts

$c0$  = refers to zero clearance case  
 $i$  = inner  
 $l$  = lower  
 $o$  = outer  
 $p$  = pressure induced (Poiseuille)  
 $s$  = shear induced (Couette)  
 $u$  = upper

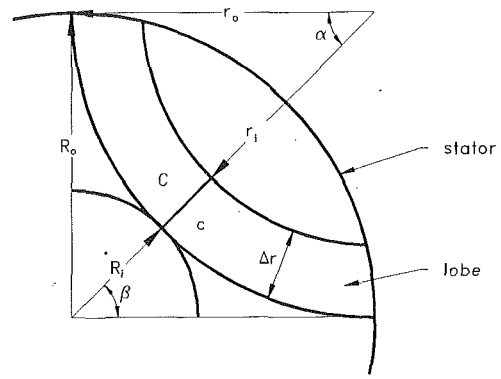


Fig. 2 Geometric variable definitions for semicircular lobe design

where  $y$  is the transverse direction. For this linear equation, the net flow can be calculated by superimposing the Couette and Poiseuille flow components.

**Semicircular Lobe Analysis.** Geometric definitions of a semicircular lobe are shown in Fig. 2, where a lobe is placed on a stationary disk (stator) having an outside radius  $R_o$ . The radius  $R_i$  represents a circle tangent to outer radius of the lobe,  $r_i + \Delta r$ . The lobes are stepped to form a large gap,  $C$ , and a small gap,  $c$ , with a flat disk rotor.

The Couette flow per unit length is given by

$$q_s = \frac{\omega R h}{2} @ R_i + \Delta r \leq R \leq R_o \quad (2)$$

and the Poiseuille flow per unit length is given by

$$q_p = -\frac{h^3}{12\mu} \frac{\partial p}{\partial r} @ r_i \leq r \leq r_o \quad (3)$$

Integrating  $q_s$  across the radial extent, and  $q_p$  along the lobes circumference and then across their width results in  $Q_s$ , and  $Q_p$ , respectively. The net flow is the superposition of these two components, i.e.,  $Q = Q_s + Q_p$ . The details of the derivation for the equation describing the pumping capability of  $n$  semicircular lobes are found in Etsion and Yaier (1988). Their resulting equation for the net flow is

$$Q = \frac{n}{4} \omega s R_o^2 \left[ 1 - \left( \frac{R_i + \Delta r}{R_o} \right)^2 \right] + \frac{n}{12\mu} (C^3 + c^3) \frac{\alpha P}{\ln \left( 1 - \frac{\Delta r}{r_o} \right)} \quad (4)$$

where  $s = C-c$  is the machined step height. The geometric constraint of lobe tangency at the outer radius requires that

$$\alpha = \frac{\pi}{2} - \beta = \frac{\pi}{2n} (n-2) \quad (5)$$

Introducing  $F_n$ , a function of the number of lobes,

$$F_n = \frac{1 - \sin\beta}{\cos\beta} = \frac{R_i}{R_o} \quad (6)$$

and a nondimensional lobe width,  $\xi = \Delta r/R_o$ , the pump flow is rewritten as (Etsion and Yaier, 1988)

$$Q = \frac{\omega s n}{4} R_o^2 [1 - (F_n + \xi)^2] + \frac{\pi P}{24\mu} (C^3 + c^3) \frac{n-2}{\ln\left(1 - \frac{\xi}{\tan\beta}\right)} \quad (7)$$

The tangency requirement of the semicircular lobe imposes a constraint on the radius  $R_i$  through Eqs. (5) and (6) once the number of lobes,  $n$ , and the outer radius  $R_o$ , have been specified.

**Semicircular Lobe Optimization.** To determine which of the two lobe designs is superior, optimization of lobe geometry for maximum flow is performed. The variables of the semicircular lobe design are the number of lobes,  $n$ , the nondimensional lobe width,  $\xi$ , and the step height,  $s$ . The step is nondimensionalized by the small clearance parameter,  $c$ , such that  $\sigma = s/c$ . In Etsion and Yaier (1988), the step height was not treated as a variable; it was defined to be a given operating condition. The step height, however, is a geometric variable and does not necessarily need to be prescribed as an operating condition. Therefore, the step height is treated in the present work as a design variable to be optimized for maximum flow. Because of the new role of the step height, this work bifurcates now from the work presented by Etsion and Yaier (1988).

An operating conditions parameter,  $S'$ , is defined by

$$S' = \frac{\pi P}{12 \mu \omega} \left(\frac{c}{R_o}\right)^2 \quad (8)$$

$S'$  contains all the variables usually specified by the design requirements of the pump. (It may be regarded to have the role of the inverse of the Sommerfeld number in journal bearings.)

The equation for flow (Eq. (7)) can be written as

$$Q = \frac{1}{2} \omega c R_o^2 Q' \quad (9)$$

where  $Q'$  is the nondimensionalized flow that includes the operating conditions parameter  $S'$  as follows:

$$Q' = \frac{\sigma n}{2} [1 - (F_n + \xi)^2] + S' [(\sigma + 1)^3 + 1] \frac{(n-2)}{\ln\left(1 - \frac{\xi}{\tan\beta}\right)} \quad (10)$$

This equation is optimized for a given operating conditions parameter,  $S'$ , by setting its partial derivatives with respect to the nondimensional lobe width,  $\xi$ , and the nondimensional step height,  $\sigma$ , equal to zero for a particular number of lobes,  $n$ . The result from  $\partial Q'/\partial \xi = 0$  is

$$S' = \frac{n\sigma(F_n + \xi) \left[ \ln\left(1 - \frac{\xi}{\tan\beta}\right) \right]^2 (\tan\beta - \xi)}{(n-2)[(\sigma+1)^3 + 1]} \quad (11)$$

The result from  $\partial Q'/\partial \sigma = 0$  is

$$S' = \frac{n[(F_n + \xi)^2 - 1] \ln\left(1 - \frac{\xi}{\tan\beta}\right)}{6(n-2)(\sigma+1)^2} \quad (12)$$

The resulting Eqs. (11) and (12) were solved simultaneously to yield the optimal values of  $\xi$  and  $\sigma$  for a specified number of lobes,  $n$ , at a given operating conditions parameter,  $S'$ . The

**Table 1 Semicircular lobe optimization results at two values of  $S'$  for various lobe numbers,  $n$**

| $S'$               | Lobes $n$ | Lobe width $\xi$ | Step height, $\sigma$ | Flow $Q'$ |
|--------------------|-----------|------------------|-----------------------|-----------|
| $1 \times 10^{-6}$ | 3         | 0.253            | 238.96                | 173.66    |
|                    | 4         | 0.194            | 211.73                | 177.54    |
|                    | 5         | 0.158            | 193.23                | 178.18*   |
|                    | 6         | 0.133            | 179.30                | 176.93    |
|                    | 7         | 0.116            | 168.20                | 174.65    |
| $1 \times 10^{-3}$ | 3         | 0.273            | 6.79                  | 4.443*    |
|                    | 4         | 0.213            | 5.96                  | 4.407     |
|                    | 5         | 0.176            | 5.40                  | 4.310     |
|                    | 6         | 0.151            | 4.97                  | 4.180     |
|                    | 7         | 0.133            | 4.63                  | 4.036     |

\*Designates maximum flow and optimal number of lobes.

**Table 2 Compilation of semicircular lobe optimization results for maximum flow**

| Parameter $S'$     | No. of lobes, $n$ | Lobe width, $\xi$ | Step height, $\sigma$ | Maximum flow, $Q'$ |
|--------------------|-------------------|-------------------|-----------------------|--------------------|
| $1 \times 10^{-6}$ | 5                 | 0.15779           | 193.23                | 178.18             |
|                    |                   | 0.15802           | 136.42                | 125.59             |
|                    |                   | 0.15819           | 111.25                | 102.29             |
|                    |                   | 0.15834           | 96.245                | 88.397             |
|                    |                   | 0.15847           | 86.005                | 78.918             |
|                    |                   | 0.15859           | 78.447                | 71.922             |
|                    |                   | 0.15870           | 72.573                | 66.484             |
|                    |                   | 0.15880           | 67.838                | 62.101             |
|                    |                   | 0.15890           | 63.915                | 58.470             |
|                    |                   | 0.15899           | 60.597                | 55.398             |
| $2 \times 10^{-5}$ | 4                 | 0.15973           | 42.631                | 38.768             |
|                    |                   | 0.16029           | 34.672                | 31.400             |
|                    |                   | 0.19689           | 32.835                | 27.013             |
|                    |                   | 0.19733           | 29.288                | 24.029             |
|                    |                   | 0.19774           | 26.670                | 21.826             |
|                    |                   | 0.19811           | 24.635                | 20.114             |
|                    |                   | 0.19846           | 22.995                | 18.734             |
|                    |                   | 0.19879           | 21.636                | 17.591             |
|                    |                   | 0.19910           | 20.487                | 16.624             |
|                    |                   | 0.20166           | 14.264                | 11.389             |
| $3 \times 10^{-4}$ | 3                 | 0.20366           | 11.507                | 9.0708             |
|                    |                   | 0.20538           | 9.8641                | 7.6889             |
|                    |                   | 0.20691           | 8.7429                | 6.7461             |
|                    |                   | 0.20833           | 7.9154                | 6.0502             |
|                    |                   | 0.26959           | 8.2698                | 5.5206             |
|                    |                   | 0.27085           | 7.6848                | 5.0943             |
|                    |                   | 0.27204           | 7.2003                | 4.7413             |
|                    |                   | 0.27318           | 6.7905                | 4.4427             |
|                    |                   | 0.28285           | 4.5723                | 2.8256             |
|                    |                   | 0.29087           | 3.5904                | 2.1090             |
| $1 \times 10^{-3}$ | 3                 | 0.29809           | 3.0055                | 1.6816             |
|                    |                   | 0.30484           | 2.6065                | 1.3896             |
|                    |                   | 0.31126           | 2.3121                | 1.1738             |
|                    |                   | 0.31746           | 2.0831                | 1.0060             |
|                    |                   | 0.32350           | 1.8985                | 0.87061            |
|                    |                   | 0.32941           | 1.7455                | 0.75836            |
|                    |                   | 0.33523           | 1.6158                | 0.66334            |
|                    |                   | 0.39208           | 0.90295               | 0.14948            |

nondimensional flow,  $Q'$ , was then computed with those  $\xi$ ,  $\sigma$ , and  $n$  values. Values for  $Q'$  were then compared over a range of  $n$  values to determine which  $n$  (and the corresponding  $\xi$  and  $\sigma$ ) yielded the maximum flow. The optimization was performed in this manner because the number of lobes must be an integer parameter.

Table 1 presents the results of the optimization for two extremes of the operating conditions parameter,  $S'$ . Table 1 reveals that the optimization of  $Q'$  is not particularly sensitive to the number of lobes, providing that the corresponding  $\xi$  and  $\sigma$  values are used. Table 2 contains the collection of those cases for which the number of lobes,  $n$ , yields maximum flow for a wide range of  $S'$  values (i.e., the collection of all "star" cases, such as in Table 1). Table 2 reveals that  $n = 5$ , and  $n = 3$  are optimal for low and high values of  $S'$ , respectively, while  $n = 4$  is optimal for intermediate values of  $S'$ . (This

finding differs from the finding by Etsion and Yaier (1988) who suggest  $n$  values greater than five.)

**Numerical Examples.** The same numerical examples as in Etsion and Yaier (1988) will be examined:

(a) *General Application*

|                          |                      |
|--------------------------|----------------------|
| Pump rotor radius, $R_o$ | 100 mm               |
| Minimum gap, $c$         | 50 $\mu\text{m}$     |
| Step height, $s$         | 50 $\mu\text{m}$     |
| Fluid viscosity, $\mu$   | 100 mPa s            |
| Pump speed, $\omega$     | 377 rad/s (3600 rpm) |
| Discharge pressure, $P$  | 1.5 MPa              |

Etsion and Yaier (1988) suggest using  $n = 5$  and  $\xi = 0.155$ . Using Eqs. (5)–(7) one obtains  $Q = 1.040 \times 10^{-4} \text{ m}^3/\text{s}$ . In the current method of optimization the step height,  $s$ , is treated as a design variable. First, the value for  $S'$  is calculated using Eq. (8) ( $S' = 2.6 \times 10^{-3}$ ). Table 2 provides for this value (using Lagrangian interpolation)  $n = 3$ ,  $\xi = 0.28778$ ,  $\sigma = 3.9144$ , and  $Q' = 2.3456$ . Thus, the step to be machined is  $s = \sigma c = 196 \mu\text{m}$ , and using Eq. (9), or Eqs. (5)–(7), the dimensional flow is  $Q = 2.211 \times 10^{-4} \text{ m}^3/\text{s}$ . The latter represents 113 percent improvement over the previous value.

(b) *Medical Application*

|                          |                      |
|--------------------------|----------------------|
| Pump rotor radius, $R_o$ | 80 mm                |
| Minimum gap, $c$         | 30 $\mu\text{m}$     |
| Step height, $s$         | 40 $\mu\text{m}$     |
| Fluid viscosity, $\mu$   | 2 mPa s              |
| Pump speed, $\omega$     | 120 rad/s (1146 rpm) |
| Discharge pressure, $P$  | 80 kPa               |

Etsion and Yaier (1988) suggest using  $n = 3$  and  $\xi = 0.27392$ . Using Eqs. (5)–(7) one obtains  $Q = 5.021 \times 10^{-6} \text{ m}^3/\text{s}$ . In the current method of optimization the same steps as above are repeated:  $S' = 1.227 \times 10^{-2}$ . Table 2 provides for this value (again using Lagrangian interpolation)  $n = 3$ ,  $\xi = 0.34822$ ,  $\sigma = 1.3820$ , and  $Q' = 0.49245$ . Thus, the step to be machined is  $s = \sigma c = 41.5 \mu\text{m}$ , and the dimensional flow is  $Q = 5.671 \times 10^{-6} \text{ m}^3/\text{s}$ . The latter represents 13 percent improvement. It is worth noting that while the step heights are very similar in both methods, improvement is due to a better lobe width selection.

It is clear from Table 2 that it is preferable to operate the pump with the smallest  $S'$  possible to generate maximum flow. One way to achieve that, according to Eq. (8), is by selecting a designed clearance,  $c$ , as small as practically possible. (In fact, the best pumping conditions are when  $c = 0$ , as will be discussed later.) It is also evident that as  $S'$  decreases the corresponding nondimensional step height,  $\sigma$ , increases, which keeps the dimensional step height,  $s$ , practical.

**Straight Lobe Analysis.** The straight lobe concept is introduced in Fig. 3. A straight symmetric V-shaped lobe is shown in Fig. 3(a) in relation to a semicircular lobe. When both lobe designs have the same radial extent (as shown) the

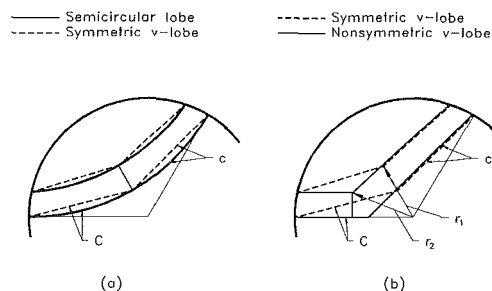


Fig. 3 Graphical comparison of lobe designs (a) symmetric V-lobe versus semicircular lobe, (b) nonsymmetric V-lobe versus symmetric V-lobe

net inward Couette flow is the same. For the symmetric V-lobes, however, the Poiseuille flow is less than the Poiseuille flow of the semicircular lobe because the symmetric V-lobe has a shorter effective length over which the fluid can flow. In other words, even when both lobe designs have the same inward flow (pumping), the straight lobe design has reduced losses. The more important advantage of the straight lobes, however, is that the radial extent (and, therefore, net inflow) is not limited by geometric tangency constraints as is the case for the semicircular lobes. The radial extent for the straight lobes could theoretically be the entire radius of the stator, thus augmenting the net inflow. These make the straight lobe a superior design.

Moreover, the straight lobe concept can be further improved. Consider Fig. 3(b) where a nonsymmetric V-lobe is shown in relation to a symmetric V-lobe. For both designs, the net inward Couette flow is the same if  $r_1 = r_2$ . The nonsymmetric V-lobe design, however, has the potential to have smaller Poiseuille flow losses than the symmetric V-lobe. The losses are proportional to the gap height raised to the third power (Eq. (3)). Because the gap between the rotor and stator for the leg of the lobe labelled  $C$  ( $C$ -leg) is larger than the gap over the leg of the gap labelled  $c$  ( $c$ -leg), the length of the  $C$ -leg should be minimized. The nonsymmetric V-lobe design accomplishes this. It is true that the losses related to the  $c$ -leg increase because this leg is now longer (which also makes the total lobe length, i.e., the length of  $c$ -leg plus the length of  $C$ -leg, for the nonsymmetric V-lobe greater than that for the symmetric V-lobe). However, the increase in losses due to this increased length varies only linearly with the length of the leg. In cases where  $C$  is sufficiently larger than  $c$ , the result will be that the nonsymmetric V-lobe overall has less flow losses, i.e., it has higher pumping capabilities than the symmetric V-lobe.

As for the semicircular lobe case, the geometries of the two straight lobe designs were optimized to achieve maximum flow. Because the nonsymmetric V-lobe did indeed turn out to be superior (see Mainland, 1990), the investigation of the symmetric V-lobe will not be presented here.

The geometry to be considered for the nonsymmetric V-lobe (hereto referred to as the V-lobe) is shown in Fig. 4. The variables are the lobe width,  $\delta$ , the step height,  $s = C - c$ , the angle,  $\alpha$ , and the number of lobes,  $n$ . The equation for net flow is found by superimposing the Couette flow component with the Poiseuille flow component. The Couette flow is found by integrating the Couette flow per unit length (Eq. (2)) for the geometry in Fig. 4. The integration is from  $R_s$  to  $R_o$  and the result is:

$$Q_s = \frac{\omega S}{4} (R_o^2 - R_s^2) \quad (13)$$

where

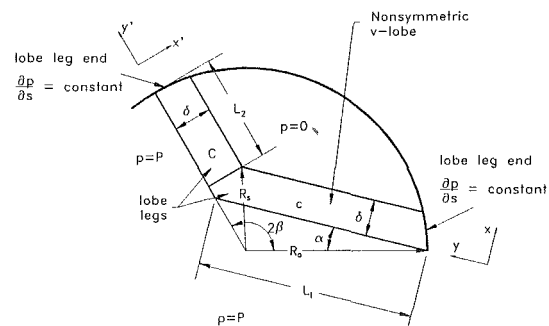


Fig. 4 Geometric variable definition and FEM boundary conditions for nonsymmetric V-lobe design

$$R_s^2 = \delta^2 + \left[ \frac{R_o \sin \alpha}{\sin(\alpha + 2\beta)} + \frac{\delta}{\tan\left(\frac{\alpha + 2\beta}{2}\right)} \right]^2 \quad (14)$$

The Poiseuille component cannot be solved exactly, so two approximations are made. It is assumed that the *c*-leg and *C*-leg have uniform lengths  $L_1$  and  $L_2$ , respectively, and the corresponding pressure gradients,  $\partial p/\partial x$  and  $\partial p/\partial x'$ , are both equal to  $P/\delta = \text{constant}$  (Fig. 4). Using the sine theorem and trigonometric identities, the lengths  $L_1$  and  $L_2$  are determined to be (Mainland, 1990)

$$L_1 = \frac{R_o \sin 2\beta}{\sin(\alpha + 2\beta)}$$

and

$$L_2 = R_o - \frac{\delta}{\tan\left(\frac{\alpha + 2\beta}{2}\right)} - \frac{R_o \sin \alpha}{\sin(\alpha + 2\beta)}$$

Integrating the Poiseuille flow per unit length (Eq. (3)), along the length of the legs,  $L_1$  and  $L_2$ , results in

$$Q_p = -\frac{C^3 P}{12\mu\delta} \left[ R_o - \frac{\delta}{\tan\psi} - \frac{R_o \sin \alpha}{\sin(\alpha + 2\beta)} \right] - \frac{c^3 P}{12\mu\delta} \left[ \frac{R_o \sin 2\beta}{\sin(\alpha + 2\beta)} \right] \quad (15)$$

where  $\psi = (\alpha + 2\beta)/2$ .  $Q_s$  and  $Q_p$  (Eqs. (13) and (15)) are added together to account for the total flow for  $n$  lobes:

$$Q = \frac{n\omega S}{4} \left( R_o^2 - \left\{ \delta^2 + \left[ \frac{R_o \sin \alpha}{\sin(\alpha + 2\beta)} + \frac{\delta}{\tan\psi} \right]^2 \right\} \right) - \frac{nP}{12\mu\delta} \left\{ C^3 \left[ R_o - \frac{\delta}{\tan\psi} - \frac{\sin \alpha}{\sin(\alpha + 2\beta)} \right] + c^3 \left[ \frac{R_o \sin 2\beta}{\sin(\alpha + 2\beta)} \right] \right\} \quad (16)$$

As in the case of the semicircular lobe design, Eqs. (8) and (9) are used to solve for  $Q'$ . For the nonsymmetric V-lobe, the dimensionless flow is

$$Q' = n \left\{ \frac{\sigma}{2} \left[ 1 - \xi^2 - \left( \frac{\sin \alpha}{\sin(\alpha + 2\beta)} + \frac{\xi}{\tan\psi} \right)^2 \right] - \frac{2S'}{\xi\pi} \left[ (1 + \sigma)^3 \left( 1 - \frac{\xi}{\tan\psi} - \frac{\sin \alpha}{\sin(\alpha + 2\beta)} \right) + \frac{\sin(2\beta)}{\sin(\alpha + 2\beta)} \right] \right\} \quad (17)$$

where  $\xi = \delta/R_o$  and  $\sigma = s/c$ .

**Nonsymmetric V-lobe Optimization.** The next step in the investigation of the nonsymmetric V-lobe is to optimize Eq. (17) with respect to the variables  $\alpha$ ,  $\xi$ ,  $\sigma$ , and  $n$ . The optimization was performed using the method of path of steepest ascent and the results are presented in Table 3. The general method of optimization was to vary the variables  $\alpha$ ,  $\sigma$ , and  $\xi$  for  $n = 3, 4, 5 \dots$  for a given operating conditions parameter,  $S'$ , to find which geometry yielded maximum flow. The results show that  $Q'$  increases as  $n$  increases and no optimal  $n$  is found. While a very large number of lobes is possible in theory, it would be impractical because there would not be sufficient room for the fluid to flow into the center of the pump. Note also that in all cases, the optimal  $\alpha$  is zero degrees. This angle,  $\alpha = 0$  provides for maximum lobe thickness,  $\delta$ , (and therefore minimum Poiseuille losses), for a given net Couette inflow. Again,  $\alpha = 0$  is not a practical value since there is no room for the fluid to exit through the center of the pump. Later, the geometry will be optimized for a practical  $\alpha$  value.

Before comparing the values for  $Q'$  in Table 3 to the values

**Table 3 Nonsymmetric V-lobe optimization results**

| $S'$               | $n$ | Lobe width, $\xi$ | Angle $\alpha$ (deg) | Step height, $\sigma$ | Flow $Q'$ |
|--------------------|-----|-------------------|----------------------|-----------------------|-----------|
| $1 \times 10^{-6}$ | 3   | 0.362             | 0.0                  | 313.3                 | 258.3     |
|                    | 4   | 0.313             | 0.0                  | 308.6                 | 330.4     |
|                    | 5   | 0.269             | 0.0                  | 296.5                 | 389.8     |
|                    | 6   | 0.234             | 0.0                  | 282.9                 | 440.7     |
|                    | 7   | 0.207             | 0.0                  | 269.6                 | 485.6     |
| $1 \times 10^{-3}$ | 3   | 0.379             | 0.0                  | 9.13                  | 6.98      |
|                    | 4   | 0.329             | 0.0                  | 9.03                  | 8.90      |
|                    | 5   | 0.284             | 0.0                  | 8.68                  | 10.43     |
|                    | 6   | 0.249             | 0.0                  | 8.23                  | 11.69     |
|                    | 7   | 0.220             | 0.0                  | 7.88                  | 12.77     |

for  $Q'$  obtained in the semicircular lobe optimization, the validity of the equations used to approximate the Poiseuille component of flow for the nonsymmetric V-lobe need to be checked. To check the validity, shape factors borrowed from heat transfer (Kreith and Bohn, 1986, and Blech et al., 1986) are used to see if the previously derived equations fell within the bounds of the possible solutions. Following this, the finite element method (FEM) is used to check the more detailed accuracy of the equations.

**Verification of V-lobe Analysis Using Shape Factors.** Shape factors are used to provide approximate analytical expressions for the flow across complex geometries, for which a closed-form solution is not feasible, or a numerical solution is not sought. The analytical expressions can be used for a quick performance prediction, preliminary design, and optimization. Here we check whether the previously derived leg lengths  $L_1$  and  $L_2$  are appropriate for the Poiseuille flow calculation over the nonsymmetric V-lobe. For  $U = 0$  the Reynolds equation (Eq. (1)) reduces to

$$\frac{\partial}{\partial x} \left( h^3 \frac{\partial p}{\partial x} \right) + \frac{\partial}{\partial y} \left( h^3 \frac{\partial p}{\partial y} \right) = 0 \quad (18)$$

The height,  $h$ , is alternately  $C$  over the short leg, and  $c$  over the long leg as in Fig. 4. Since  $h$  is constant over each of the legs, Eq. (18) reduces to the Laplace equation,  $\nabla^2 p = 0$ . For the geometry being considered the pressure is governed by the Laplace equation with Dirichlet boundary conditions over one portion of the boundaries, and homogeneous Neumann conditions over the remaining boundaries (leg ends). It is apparent that the Poiseuille flow problem is analogous to the heat flow problem: the potential is the pressure  $p$ , the conductance is  $h^3/12\mu$ , and the flow is the fluid flow. The shape factor, which is determined solely by geometry, is the same as in the heat transfer problem. The upper bound is found by assuming isobars, which are analogous to isotherms. The lower bound is found by assuming streamlines, which are analogous to adiabats. A formal proof of the validity of the bounds is given in Mainland (1990).

For the Poiseuille flow over the V-lobes, each of the lobe legs can be generically described by the geometry of Fig. 5. Although one end of each lobe leg is an arc, it will be approximated as a secant. The upper bound shape factor is found in reference to Fig. 5(a) to be (Mainland (1990)):

$$S_u = \frac{\tan \alpha + \tan \beta}{\ln \left( \frac{L}{L - D(\tan \alpha + \tan \beta)} \right)} \quad (19)$$

and the lower bound shape factor is found using the variables of Fig. 5(b):

$$S_l = \frac{\alpha + \beta}{\ln \left( \frac{L}{L - D(\tan \alpha + \tan \beta)} \right)} \quad (20)$$

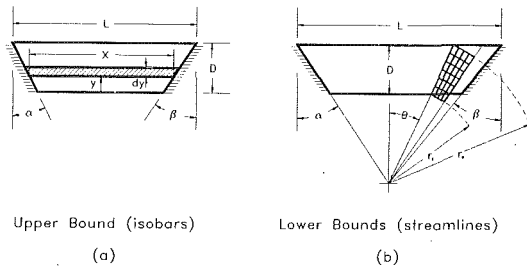


Fig. 5 Generic V-lobe geometry for shape factors (a) upper bound, (b) lower bound

Now upper and lower bounds for Poiseuille flow can be calculated by:

$$(Q_p)_{u/l} = K S_{u/l} \Delta p; @ K = \frac{h^3}{12\mu} \quad (21)$$

where  $K$  is the conductance.

The equation for Couette flow (which was obtained in closed-form (Eq. (13)) was used with the bounded Poiseuille flows to account for the bounded total flows. Specified operating conditions were selected based on possible operating conditions for the pump, though any set of conditions could be used. Figure 6 shows that the equation for flow of the nonsymmetric V-lobe (Eq. (16)) predicts pump performance very close to the flows predicted using the bounds. Note that  $S_u$  represents an upper bound for the Poiseuille flow, and, therefore, a lower bound for the total flow. Although the results from the equation are slightly out of the range predicted by the bounds the variation is negligible.

**Verification of V-lobe Analysis Using Finite Element Method.** The finite element model can only be solved for a given geometry, i.e., it cannot be used to arrive at an optimal geometry unless the optimization process is done on a case by case basis. The finite element model was solved over a range of geometries for the nonsymmetric V-lobe configuration. A detailed formulation appears in Mainland (1990).

A fluid film height ratio of  $C/c = 6$  (or  $\sigma = 5$ ) was selected for the FEM model. The optimization of the pump equations yielded values in this range and higher (see Table 3). The lower end value of six was selected instead of a higher value so that the contribution to the flow across the  $c$ -leg could be examined.

The boundary conditions are  $p = P$  along the lower edge of the lobe, and  $p = 0$  along the upper edge of the lobe, as shown in Fig. 4. Along the lobe ends it was assumed that the pressure varies linearly, i.e.,  $\partial p / \partial s = \text{constant}$  ( $s$  being the path along the ends of the legs). This closely simulates the condition of no flow across the lobe ends. (Any flow that does cross these boundaries is a loss that would make the pump less than optimal.)

The FEM model was solved for the full range of optimal values of  $n$ ,  $\delta/R_0$  and  $L/R_0$  encountered (Mainland, 1990). Once the pressure field was solved, the flow was calculated. A comparison between the Poiseuille flows predicted by Eq. (15) and by the FEM model reveals a difference of less than three percent throughout. It is concluded that Eq. (16) (which contains Eq. (15)) predicts the flow quite accurately, despite the approximations made with regard to the  $c$ -leg and  $C$ -leg having uniform lengths  $L_1$  and  $L_2$ , respectively.

### Comparison of Lobe Designs

**Complete Optimal Case.** The investigation above for the semicircular lobe and the V-lobe designs is based on optimal boundary conditions (no flow) at the lobe ends. These boundary conditions will be maintained throughout this work. The optimization results for the semicircular and V-lobes, as pre-

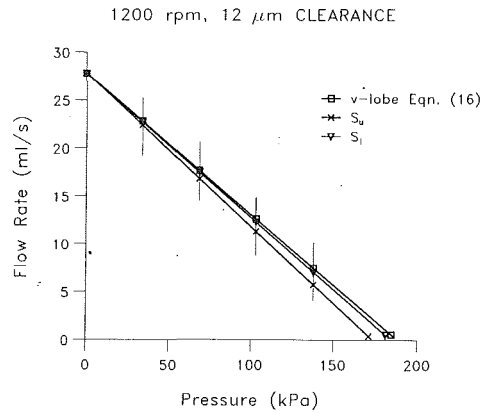


Fig. 6 Comparison of flow predicted by bounds to flow predicted by analysis

sented in Tables 1 and 3, respectively, were obtained assuming that a small clearance,  $c$ , exists. However, it can easily be verified from Eqs. (4) and (16), that maximum flow occurs when  $c = 0$  (i.e., minimum Poiseuille flow losses). Thus, of all possible values of  $c$  the zero clearance condition theoretically results in the greatest pumping capacity, i.e., an ultimate upper bound for maximum flow to which any other pump can be compared. (Because the lobes and rotor are in full contact at zero clearance it is not recommended, however, to operate the pump under this condition. Practically, a minimal clearance should be set subject to system limitations such as rotor runout, misalignment, surface roughness, and maximum particle size in the fluid being pumped.)

The equations to be optimized for  $c = 0$  must be altered slightly from the previous optimization. This is because nondimensionalizing  $s$  by  $c$  ( $\sigma = s/c$ ) is no longer appropriate. Hence, the following nondimensional parameters are used:

$$\sigma_{c0} = \frac{s}{R_0}; S'_{c0} = \frac{\pi P}{12 \mu \omega}; Q'_{c0} = \frac{1}{2} \omega R_0^3 Q_{c0} \quad (22)$$

where  $s$  is nondimensionalized by  $R_0$ ,  $S'_{c0}$  is a new version of the operation conditions parameter,  $S'$ , and a new dimensionless flow,  $Q'_{c0}$  is defined from  $Q_{c0}$  being the flow,  $Q$ , when the clearance is zero. Using these definitions, the dimensionless equation for flow at  $c = 0$  is

$$Q'_{c0} = \frac{\sigma n}{2} [1 - (F_n + \xi)^2] + S'_{c0} \sigma_{c0}^3 \frac{(n-2)}{\ln \left( 1 - \frac{\xi}{\tan \beta} \right)} \quad (23)$$

for the semicircular lobe (from Eq. (7)), and

$$Q'_{c0} = \frac{\sigma_{c0} n}{2} \left[ 1 - \xi^2 - \left( \frac{\sin \alpha}{\sin(\alpha + 2\beta)} + \frac{\xi}{\tan \psi} \right)^2 \right] - S'_{c0} \frac{2n}{\pi \xi} \sigma_{c0}^3 \left[ 1 - \frac{\xi}{\tan \psi} - \frac{\sin \alpha}{\sin(\alpha + 2\beta)} \right] \quad (24)$$

for the nonsymmetric V-lobe (from Eq. (16)).

These equations were optimized using the path of steepest ascent method. Table 4 shows a representative comparison of the results of the optimization. The V-lobe design outperforms the semicircular design for the complete optimal case. The optimal geometry occurs at  $n = 5$  for the semicircular lobe design, while  $Q'_{c0}$  continues to increase with  $n$  for the V-lobe design (this is consistent with the results for small  $S'$  in Tables 2 and 3, respectively).

**Practical Optimal Case.** The investigation of the complete optimal case above, as well as the results in Tables 1 and 3, demonstrate that the V-lobes have greater potential than the semicircular lobes. The above optimized results for the V-lobes, however, produce  $\alpha = 0$ . This means that the lobes are con-

**Table 4 Optimal pumping comparison for complete optimal case**

| $S'_{c0}$          | $n$ | $Q'_{c0}$ semic | $Q'_{c0}$ V-lobe | $Q'_{c0} V/Q'_{c0}S$ |
|--------------------|-----|-----------------|------------------|----------------------|
| $1 \times 10^{-6}$ | 3   | 5.526           | 8.206            | 1.48                 |
|                    | 5   | 5.678*          | 12.389           | 2.18                 |
|                    | 8   | 5.484           | 16.736           | 3.05                 |
| $1 \times 10^{-3}$ | 3   | 174.8           | 259.5            | 1.48                 |
|                    | 5   | 179.6*          | 391.8            | 2.18                 |
|                    | 8   | 173.4           | 529.2            | 3.05                 |

\*Designates maximum flow and optimal number of lobes.

**Table 5 Optimal pumping comparison for a practical angle  $\alpha = 11.54$  deg**

| $S'$               | $n$ | $Q'$              |                     |
|--------------------|-----|-------------------|---------------------|
|                    |     | Semicircular lobe | Nonsymmetric V-lobe |
| $1 \times 10^{-6}$ | 3   | 173.66            | 233.46              |
|                    | 5   | 178.18*           | 350.22              |
|                    | 7   | 174.65            | 432.09              |
|                    | 9   | 171.81            | 467.36              |
| $1 \times 10^{-3}$ | 3   | 4.443*            | 6.315               |
|                    | 5   | 4.310             | 9.337               |
|                    | 7   | 4.036             | 11.304              |
|                    | 9   | 3.888             | 12.108              |

\*Designates maximum flow and optimal number of lobes.

tiguous and there is no room at the center of the pump for the fluid to exit. In practice an exit hole must exist and its radius should be large enough to minimize resistance to outflow. It should be noted, however, that the exit hole can undercut the lobes from beneath, subject to the constraint that its radius,  $R_h$ , does not reach the low pressure zone. Referring to Fig. 2 for the semicircular lobes,  $R_h < R_i + \Delta r$ , and to Fig. 4 for the V-lobes,  $R_h < R_o \sin \alpha + \delta$ . Practically, these conditions are not very restrictive because of the additional space that  $\Delta r$  and  $\delta$  provide.

An angle  $\alpha$  greater than zero imposes a constraint on the optimization process. Therefore, the value of maximum  $Q'$  decreases as  $\alpha$  increases. The following is a check to ensure that even when  $\alpha$  takes on a physically reasonable value, the V-lobe design still outperforms the semicircular lobe design. For this check also the small clearance,  $c$ , is nonzero.

A generous angle  $\alpha = 11.54$  deg (which corresponds to  $R_h = 0.2R_o$ ) was selected to provide a wide separation between lobes. Table 5 lists a comparison between the optimal  $Q'$  values for the semicircular and V-lobes at two extreme values of  $S'$ . Table 5 proves again that the V-lobe design provides a more efficient pumping mechanism even when  $\alpha$  takes on a non-optimal value. (Note in Table 5 that the  $Q'$  values for the nonsymmetrical V-lobes are lower than those in Table 3, as expected. Hence, one should always attempt to design with the smallest  $\alpha$  possible.)

### Conclusions and Recommendations

Both a semicircular lobe and a new V-lobe viscous pump have been analytically investigated. The analysis was performed using several approaches. The solution for the semicircular lobe is exact (it is based on closed form integration (Etsion and Yaier, 1988)). For the V-lobe, however, a closed form solution does not exist. An analytical model is provided based on reasonable approximations. The approximations are

validated using shape factors and finite element models. For both lobe designs, pump geometry is optimized for maximum pumping capacity. The results of the optimization show that the V-lobe produces a superior pumping mechanism to the semicircular lobe.

The V-lobes have two major advantages over the semicircular lobe. The first is that simply making the lobes straight, as opposed to being curved, reduces the pumping losses. The second, and most important advantage, is that the radial extent of the V-lobes and the number of lobes, are not limited by geometry constraints (such as the tangency requirement of the semicircular lobes). For the straight lobes, pumping capacity increases with the number of lobes and the radial extent.

Increased pumping capacity could be realized by locating the rotor between two stators. This is equivalent to operating two pumps in parallel. Further improvements could probably be made on the lobe leg configuration such as variable lobe width and step height along the length of the lobe legs. Modifications of this nature, however, would be made at the cost of increased manufacturing complexity. The optimization here was performed on the basis of maximizing the flow rate,  $Q$ . An alternate optimization could have been performed to maximize the pressure.

### Acknowledgments

This project was supported in part by a Georgia Tech Foundation Grant, E25-549, made by Mr. Gilbert Bachman, and by the Department of Defense, National Defense Science and Engineering Graduate Fellowship Program, under the sponsorship of the Air Force. This support is gratefully acknowledged.

### References

- Blech, J. J., Green, I., and Kopelman, J., 1986, "Transient Temperature Distribution in Partially Filled Rotating Horizontal Cylinders," *ASME Journal of Applied Mechanics*, Vol. 53, No. 2.
- Etsion, I., 1984, "A New Concept of Zero-Leakage Noncontacting Mechanical Face Seal," *ASME JOURNAL OF TRIBOLOGY*, Vol. 106, No. 3, pp. 338-343.
- Etsion, I., and Yaier, R., 1988, "Performance Analysis of a New Concept Viscous Pump," *ASME JOURNAL OF TRIBOLOGY*, Vol. 110, No. 1, pp. 93-99.
- Green, I., Mainland, M., and Etsion, I., 1990, "Experimental Investigation of a New Concept Viscous Pump," *ASME JOURNAL OF TRIBOLOGY*, preprint 90-Trib-58.
- Hasinger, S. H., and Kehrt, L. G., 1963, "Investigation of a Shear-Force Pump," *ASME Journal of Engineering for Power*, Vol. 85, pp. 201-207.
- Hsing, F. C., 1972, "Formulation of a Generalized Narrow Groove Theory for Spiral Grooved Viscous Pumps," *ASME JOURNAL OF LUBRICATION TECHNOLOGY*, Vol. 94, No. 1, pp. 81-85.
- Hsing, F. C., 1974, "Analytical Solutions for Incompressible Spiral Groove Viscous Pumps," *ASME JOURNAL OF LUBRICATION TECHNOLOGY*, Vol. 96, No. 3, pp. 365-369.
- Kreith, F., and Bohn, M. S., 1986, *Principles of Heat Transfer*, 4th ed., Harper and Row Publishers, New York, pp. 89-94.
- Mainland, M. E., 1990, "Analytical and Experimental Investigation of an Efficient Viscous Pump," M.S. thesis, Georgia Institute of Technology, Atlanta, Georgia.
- Missimer, J. R., and Johnson, W. S., 1982, "Flow Between a Smooth Stationary Disk and Grooved Rotating Disk," *ASME JOURNAL OF LUBRICATION TECHNOLOGY*, Vol. 104, pp. 248-254.
- Sato, Y., Ono, K., and Moriguchi, N., 1988, "Analysis of Viscous Pumps With Shrouded Rayleigh-Steps Using Compressible Fluid," *ASME Paper No. 88-Trib-44*.
- Sato, Y., Ono, K., and Iwana, A., 1990, "The Optimum Groove Geometry for Spiral Groove Viscous Pumps," *ASME JOURNAL OF TRIBOLOGY*, Vol. 112, No. 2, pp. 409-414.
- Vohr, J. H., and Pan, C. H. T., 1968, "Gas-Lubricated Spin-Axis Bearings for Gyroscopes," MTI-68TR29, Mechanical Technology Incorporated, Latham, N.Y.